# Design, Fabrication, and Testing of Plain Concrete Beams Using Topology Optimization

by
Jackson Jewett

B.A. Cognitive Science
University of California, Berkeley, 2013

SUBMITTED TO THE DEPARTMENT OF CIVIL AND ENVIRONMENTAL ENGINEERING IN PARTIAL FULFILLMENT OF THE REQUIREMENTS FOR THE DEGREE OF

MASTER OF ENGINEERING IN CIVIL AND ENVIRONMENTAL ENGINEERING
AT THE
MASSACHUSETTS INSTITUTE OF TECHNOLOGY

September 2018



Signature of Author: Signature redacted
Department of Civil and Environmental Engineering
August 14, 2018

Certified by: Signature redacted
Josephine Voigt Carstensen
Lecturer of Architecture and Civil and Environmental Engineering
Thesis Supervisor

Accepted by: Signature redacted
Heidi Nepf
Professor of Civil and Environmental Engineering
Chair, Graduate Program Committee

# Design, Fabrication, and Testing of Plain Concrete Beams Using Topology Optimization

by
Jackson Jewett

Submitted to the Department of Civil and Environmental Engineering
On August 14, 2018 in Partial fulfillment of the
requirements for the Degree of Master of Engineering in
Civil and Environmental Engineering

## ABSTRACT

Topology optimization is a structural design tool that can autonomously generate efficient forms within a design domain by ascribing fabrication material to key locations of a structure while removing it from underutilized areas. It has been known to lead to new design solutions that outperform conventional low-weight designs. This has made topology optimization a popular design tool for a wide range of applications, but examples related to civil structures such as buildings, bridges, or infrastructure remain limited. This is partly because topology optimization is a free-form design technique, and often produces complex, non-linear designs that would be difficult to fabricate on a buildings-scale. However, this tendency suggests that concrete could be an excellent building material for topology-optimized civil structures, since its initial liquid phase makes it highly formable, and it's low cost and high strength make it a ubiquitous construction material.

Materially-specific topology optimization algorithms have been suggested to account for the anisotropic behavior of reinforced concrete, however they have focused on developing strut-and-tie models and improving the damage strength of the design. At current, the validity of these algorithms remains uncertain as no designs have yet been fabricated and tested. This thesis therefore presents tests of plain concrete members designed using two different topology optimization algorithms that make different assumptions about the fabrication material's behavior, and compares their performance. Although plain concrete is rarely used on a structural scale, these initial experiments were designed without reinforcement to more clearly observe how these design algorithms reckon with the complex behavior of concrete.

It was found that an algorithm specifically programmed to optimize plain concrete designed specimens that failed at lower maximum forces than beams designed with an algorithm that was not materially specific. It is likely that this result is due to optimization output rounding that was necessary to produce manufacturable designs. The information obtained from these tests is intended to inform topology optimization algorithms of reinforced concrete in future research.

Thesis Supervisor: Josephine Voigt Carstensen
Title: Lecturer of Architecture and Civil and Environmental Engineering

# Acknowledgements

First, I would like to thank Professor John Ochsendorf, who I think took an extraordinary risk in accepting me into this program, and took extra time to convince me to accept the invitation. I am so grateful for this opportunity you have given me, and I hope we have made you proud.

I want to thank my parents, who have encouraged to pursue this career through risk and uncertainty, and who have surrounded me with love and support my entire life.

I want to thank my lifelong friends, Zack, Phil, and Luke, and Katie, Matt, and Jbear, Jill, and my roommates Ross, Ashley, and Haley. All of you helped with my applications, put up with my stress, and answered my calls when I needed you. I am lucky to have such exemplary friends.

I want to thank the people in Berkeley who helped me get here. My peers Ashley Cronk, Aaron, and Ash, and my professors, whom I admire deeply, Professor Crysler, Professor Sullivan, Professor Moehle, Profesor Astaneh-Asl, and Professor Fillipou.

I want to thank all of my MEng peers, especially Sean and Alex, who assisted me with these experiments. I could not have poured my concrete without their help.

I am so grateful to the people at MIT who helped me realize these experiments. Jen and Chris helped me make my samples, Jeanette and Kathleen kept me reimbursed and laughing, Michael Tarkanian helped a me bend steel in the blacksmithing lab, and Sarah and Kiley made sure I graduated. Steve, you were so patient, caring, and helpful all year, no matter how many times I bothered you, and you always had the solution to my problems somewhere in the basement.

The Professors at MIT, especially, I am grateful for. Professor Ulm and Admir, who gave me advice on concrete, Professor Buyukozturk, with whom I could discuss concrete for hours, and Caitlin, who has assembled a team of researchers from whom I've learned enormously, and who I can always trust to have a better idea than my own, as well as the means to make it happen.

Without doubt, this research would never have happened without my advisor, Josephine Carstensen. Josephine has been an academic wizard and a mentor, giving professional and emotional support to our entire cohort all year. You have been a role model and a leader for us, personally and professionally. It has been a privilege to work with you.

Last, I want to thank my partner, Julia Irwin, who kept me alive, supported, and opened my eyes to connections across disciplines I never could have seen on my own.

Last, thank you to the reader. I hope you build something exciting.

# Table of Contents

# List of Figures

# List of Tables

# Introduction

Topology optimization is a design framework known to generate efficient and innovative designs that typically outperform the performance of traditional low-weight structures (Sigmund & Bendsoe, 2004). The technology has already impacted the design of numerous industries around the world, such as the automotive and aerospace sectors (Zhu, Zhang, & Xia, 2016) (Cavazzuti, et al., 2011). However, topology optimization has yet to make a significant impact on civil or structural engineering disciplines. The reasons for this are numerous, but this thesis will focus specifically on the problem of manufacturability. Topology optimization often produces designs that are complex, irregular, and non-linear, such as the design in Figure 1, which shows a typical example of the complex forms generated by topology optimization. These outputs can be problematic for civil engineering applications, which tend to design large, buildings-scale structures with rectilinear components.

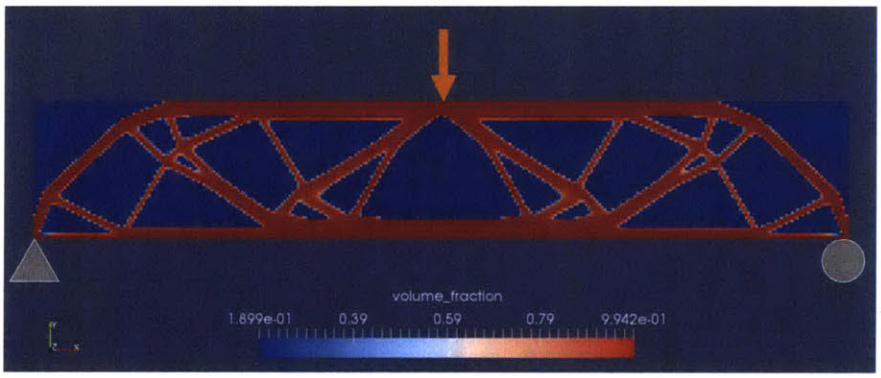


*Figure 1: Typical output of topology optimization for three-point bending beam minimizing compliance with volume constraint*

Additive manufacturing has been investigated as a possible solution to the manufacturability problem of complex forms, and example of which can be seen in Figure 2 (Zegard & Paulino, 2016) (Gaynor & Guest, 2016). Although this technology allows for the mass fabrication of small components that can take on almost any shape, it is unlikely that a 3D printer will construct a steel-framed skyscraper in the foreseeable future. Rather, it is essential to consider how to build civil-scale structures like bridges and buildings if designing them with topology optimization.

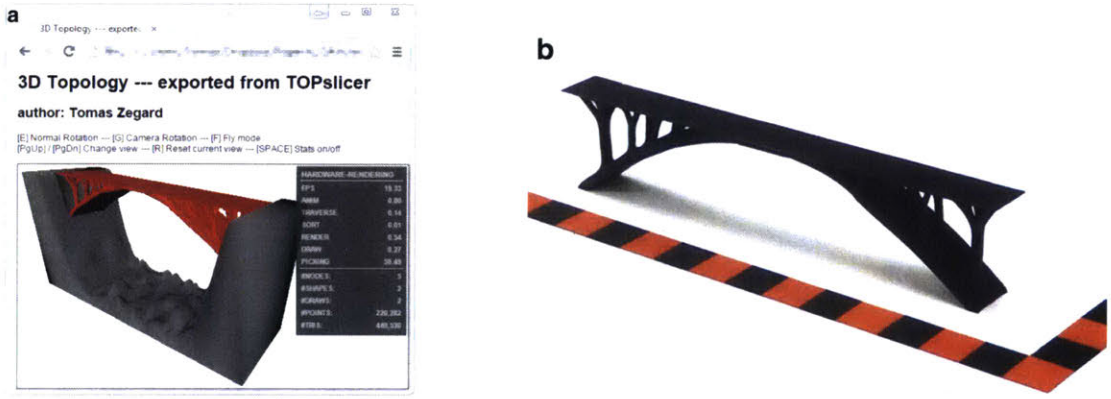


*Figure 2: Examples of topology optimized bridge, and 3D printed design; borrowed from Tomas Zegard in Structural and Multidisciplinary Optimization Journal (Zegard & Paulino, 2016)*

Very few examples of civil structures exist that were designed with topology optimization. One building though, the Qatar National Convention Center (QNCC), provides an interesting case study of how large, optimized structures have actually been built. The QNCC was designed by architect Arata Isozaki, but the feature façade was designed with inspiration from a Bi-Directional Evolutionary Structural Optimization (BESO) routine, a common approach to topology optimization (Dapogny, et al., 2017). This particular design was generated by Matsuro Sasaki. The structure projects a grand, seemingly organic, tree-like design in the desert of Doha. The structural design is supposed to be materially efficient (Sasaki, 2007) and, as can be seen in Figure 3, aesthetically impressive.

*Figure 3: Façade of the Qatar National Convention Center; photo borrowed from Nelson Garrido*

Although the structural system in this façade appears to be curving and non-linear, close inspection of the construction photos shown in Figure 4 tells a different story. In fact, the façade is actually built from a series of straight, octagonal steel elements, with a non-structural cladding affixed to the enormous beams (Januszkiewicz & Banachowicz, 2017). This construction method gives the appearance of an optimized structure, when in fact is built using conventional, prismatic elements that fail to truly capture the intent of the optimization output. Rather, curves are interpreted as lines, and the built structure undoubtedly performs differently than Sasaki's initial optimization had anticipated.

*Figure 4: Qatar National Convention Center under construction; photos borrowed from Matsuro Sasaki*

An interesting alternative opportunity for construction of civil structures designed with topology optimization may be the use of concrete as a construction material. Concrete is moldable, strong, inexpensive, and ubiquitous in the building industry (Mehta & Monteiro, 2004). Due to its initial liquid phase, it can take on virtually any shape, which could help it address the problem of accurate manufacturability for civil-scale structures. Figure 5 illustrates an example of elegantly curved concrete elements cured in an elastic flexible formwork (Culver, Koerner, & Sarafian, 2016).

*Figure 5: Curved concrete made from flexible formworks; image borrowed from Ron Culver, Julia Koerner, and Joseph Sarafian (Culver, Koerner, & Sarafian, 2016)*

However, concrete in an extraordinarily complex material, and thus requires careful attention if optimization algorithms are to be used in its design. Of particular concern is the anisotropic nature of concrete. Unlike steel, concrete behaves drastically different in tension and compression (Nilson, Darwin, & Dolan, 2008). A topology optimization algorithm that seeks to design concrete must be able to account for concrete's specific material behavior in its optimization routine, to ensure it is designing a properly functioning structure.

Several researchers have developed topology optimization codes specifically for concrete design, which shall be discussed in the following section. However, none of these algorithms have been used to build physical specimens of their designs, and none have been tested under laboratory conditions to demonstrate their accuracy or efficacy. It is the goal of this thesis to develop a topology optimization code for the design of plain concrete structures, build these structures, and test them.

For this thesis, an experiment was conducted to compare the performance of a concrete-specific algorithm to an algorithm assuming isotropic material behavior. Specimens were designed with two different optimizers under the same load case, then built and tested under laboratory conditions. Their performance was compared to the predictions of our computational models, and the results will be used for the improvement of future topology optimization algorithms.

# Literature Review

This review will focus on research related to shaping concrete beams for improved performance, and topology optimization algorithms for concrete design. There is a body of research on techniques to optimize reinforced concrete elements within code-based, prismatic parameters. A thorough review of this work is outside the scope of this paper, as here the primary interest is altering the shape and layout of the beams themselves.

Several researchers have explored the opportunities afforded by flexible formworks in shaping more efficient concrete structural elements. West has promoted the use of fabric formed concrete for optimized concrete design, often for efficient beam design (West, 2016). Orr has done extensive analysis and testing on fabric formed concrete, and pursued efficient layout of beams by modulating the depth along its length to match the moment diagram (Orr, Darby, Ibell, & Evernden, 2011), while Garbett proposed a fabric-formed optimized beam design by varying the cross-sectional profiles (Garbett, Darby, & Ibell, 2016), whose specimens are shown under stress tests in Figure 6. These optimizations involved checking the forces acting on the beam at regular intervals, and sizing the cross-section to accommodate the maximum forces. As an extension, Veenendaal applied evolutionary optimization techniques to the manufacturing constraints of fabric formed concrete to produce efficient beams that could be built with fabric formwork (Veenendaal, Coenders, Vambersky, & West, 2011).

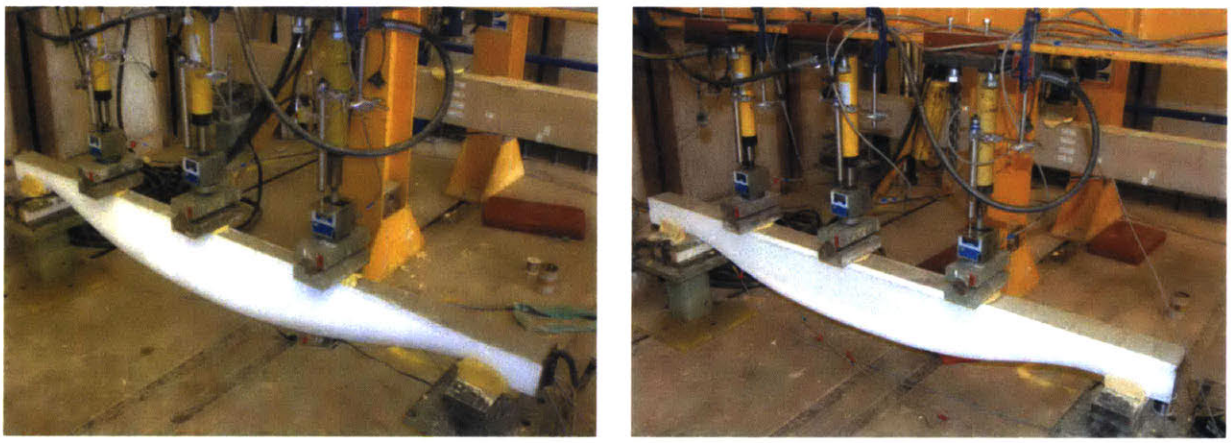

*Figure 6: Testing of optimized fabric-formed beams; image borrowed from J. Garbett (Garbett, Darby, & Ibell, 2016)*

Form-finding has also been used to make concrete structures that maintain compression-only stress conditions, which allows them to accommodate large forces with less material and no rebar. Block has used form-finding techniques to design a pure-compression floor slab design, as well as a pure-compression shell

using a flexible cable-net formwork (A. Liew, 2017) (Van Mele T., 2018). Hawkins used a similar approach, comparing examples of form-finding vaults with analytical models, to generate funicular floor slab designs with steel tension ties (Hawkins, Orr, Shepherd, Ibell, & Bregulla, 2017).

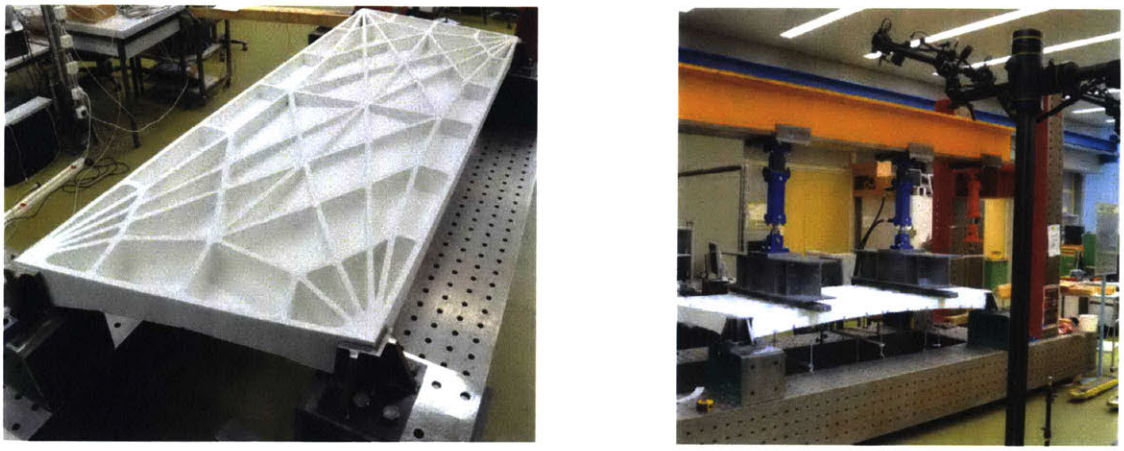

*Figure 7: Testing of pure-compression slab designed with form-finding*

Research on topology optimization of concrete has begun to gain interest. One common use is to design efficient layout of reinforcing steel for strut-and-tie concrete design. Liang first proposed this methodology, using continuum topology optimization with an evolutionary method to visualize forth paths for rebar layout (Liang, Xie, & Steven, 2000). The continuum output was interpreted as compressive and tensile truss elements for strut-and-tie design. This work was later expanded to a formulation based on the density-based topology optimization approach (Matteo Bruggi, 2012). Algorithms have been developed that could assign different material behavior to multiple materials within continuum, accounting for the different material properties of concrete and steel (Bogomolny & Amir, 2012) (Victoria, Querin, & Martí, 2011) In another area of study, continuum material that can act with compressive force is combined with a ground structure of truss elements that can accept tensile force, creating a bi-linear truss-continuum topology optimization that can offer a realistic design space for reinforced concrete design, as illustrated in Figure 8 (Gaynor, Guest, & Moen, 2013) (Bruggi, 2016) (Yang, Moen, & Guest, 2014). This concept was expanded by taking non-linearities into account based on concrete damage (Amir & Sigmund, 2013). Recently, a methodology for topology optimization of post-tensioned concrete has been introduced, as well (Amir & Shakour, 2018).

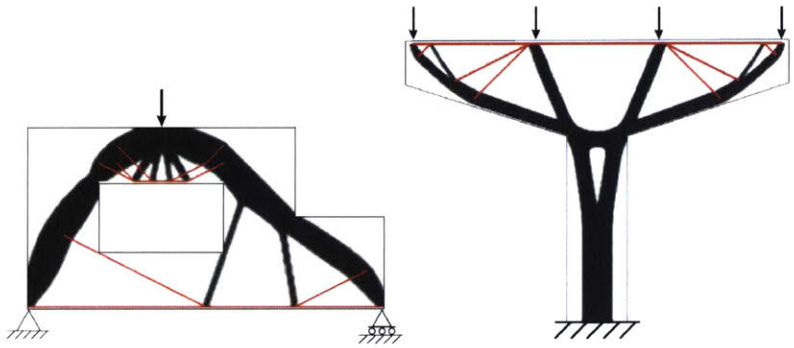

*Figure 8: Optimized strut-and-tie layout with combined truss and continuum ground structure; borrowed from Andrew T. Gaynor and James Guest (Gaynor & Guest, 2016)*

Two projects are known to have been built using topology optimization for concrete design. The first is the Unikbeton frame by Søndergaard (Dombernowski & Søndergaard, 2012), which was designed with Altair's commercial topology optimization software Optistruct 9.0 and built by milling the mold from styrofoam using a 6-axis milling robot. The optimization procedure was not concrete-specific. Rather, the construction material was assumed to be isotropic for the initial design phase, and steel was added to the design to compensate for tensile forces in the system. Additionally, Dillenburger designed and fabricated two floor slabs using 3D printed formwork and fiber-reinforced ultra-high performance concrete (Jipa, Bernhard, Dillenburger, & Aghaei-Meibodi, 2016). One slab used an ESO plug-in for Grasshopper called Millipede, while the other used a density-based algorithm of SIMULIA Abaqus. Both of these slabs assumed the material would behave isotropically, which may be reasonable for the UHP fiber-reinforced concrete used in the final designs. However, none of these structures were tested to evaluate if the physical specimens behaved as the computational models had predicted.

*Figure 9: Built concrete structures designed with topology optimization*

Although many topology optimization algorithms have been written to optimize the design of reinforced concrete structural elements, no publications have outlined the fabrication and testing of these

various approaches to concrete design. In order for topology optimization to be embraced as a viable design method for real-world concrete structures, it is essential that these algorithms be tested with physical specimens to prove their utility in concrete design.

# Methodology

The purpose of this thesis was to administer an experiment in which concrete specimens could be designed, fabricated, and tested using a materially specific topology optimization algorithm. Therefore, the methodology shall be presented in 5 subsections. First, the principles of topology optimization shall be discussed. The following sections will describe the design of the materially-specific topology optimization algorithm, the design of the structures themselves, the fabrication of the structures, and the testing of the structures.

### Topology Optimization

Topology optimization, as developed by Bendsoe and Kikuchi in their landmark 1988 paper, relies on a density based approach for structural optimization (Bendsoe & Kikuchi, 1988). Although a thorough review of the principles of topology optimization are outside the scope of this thesis, readers are referred to the 2004 book by Bendsoe and Sigmund for additional context (Bendsoe & Sigmund, 2004).

As a brief introduction to a typical topology optimization problem, a design space is divided into a mesh of finite elements, each of which has a local stiffness $K^e$. Each element is assigned a density variable $\rho^e$, and a design variable $\phi^e$ that can be controlled by an optimizer. The value of $\rho^e$ influences the stiffness of the corresponding stiffness matrix, such that higher values of $\rho^e$ mean the element is stiffer, and lower values mean it is more compliant. The value of $\rho^e$ is usually constrained between 0 and 1, and is exponentiated to a value $\eta$ to penalize non-binary values. This process is known as Solid Isotropic Material with Penalization (SIMP), and is a popular and efficient approach to topology optimization.

The value of $\rho^e$ is controlled by the design variables, $\phi^e$, whose values influence the values of the density variables within a prescribed distance away from them. Utilizing this radius of influence is known as filtering, and helps ensure smooth outputs from the optimization.

Filtering can produce non-binary densities at the interfaces of its designs, so a regularized Heaviside step function is often employed to enforce elements to have a density of either 0 or 1 (Guest, Prévost, & Belytschko, 2004). The Heaviside Projection Method (HPM) also allows designers to control the length-scale of the members in optimization outputs. HPM is modulated by an exponentiated variable, β, similarly to how ρ is modulated by η.

By influencing the values of the density variables, ρ, between 1 and 0, topology optimization is able to determine where to put material and where to remove it, in order to generate a structure optimized for a specific criteria, known as the objective function. The objective function can, for example, be to minimize the volume of the system, maximize the stiffness, or minimize the cost, among another goals. The optimization is also programmed to operate within a set of constraints given by the designer, which helps guide the algorithm towards useful outputs. Constraints could be any number of considerations, like a maximum material volume, or a maximum deflection, but one constraint is always to enforce structural equilibrium, to ensure stability, and that a finite element analysis can be solved.

Objective functions and constraints are formulated such that they are differentiable, so they can be used in a gradient-based optimizer like the Method of Moving Asymptotes, which is the optimizer used in the formulations for this thesis (Svanberg, 1987). Deriving these sensitivities allows the optimization process to happen faster.

The original application of topology optimization, and one that continues to be incredibly popular today, is to minimize the compliance of a structural system, while respecting a maximum volume constraint. Below is the formulation of this approach, that shall be referred to as a compliance-based topology optimization:

$$
\begin{aligned}
\underset{\phi}{\text{minimize}} \quad & f = \mathbf{F}^{\mathbf{T}}\mathbf{d} \\
\text{subject to} \quad & \mathbf{K}(\rho^e)\mathbf{d} - \mathbf{F} = \mathbf{0} \\
& \sum_{e \in \Omega} \rho^e v^e \leq V \\
& \phi_{min} \leq \phi_i \leq \phi_{max} \quad \forall\, i \in \Omega
\end{aligned}
$$

The first line of the formalization outlines the objective function, which is the compliance of the system. Compliance is measured as the sum of the forces, F, acting on the system multiplied by the displacements at the location of the forces, d.

The second, third, and fourth lines are the constraints on the optimization. The first constraint enforces static equilibrium, where K is the stiffness matrix and $\rho^e$ is the density variable matrix. This is done such that there is no acceleration in the system, and an FEM analysis can be conducted. The second is the volume constraint, which stops the optimizer from filling the entire design space with construction material. Finally, the last line designates the bounds of the density variables, which is typically set between 0 and 1.

**Algorithm Design:**

The above formulation, it would seem, is insufficient to be used for the optimization of concrete structures. In particular, it assumes that the fabrication material behaves isotopically, which concrete does not. Indeed, the "IM" in "SIMP" stands for "isotropic material." Outputs from this formulation could call for slender members in tension, such as that of Figure 1, that would fracture quite quickly if built out of concrete. In order to build a topology optimization algorithm for plain concrete structures, then, it was essential to capture concrete's anisotropic behavior in the structural analysis.

Concrete behavior has been studied for decades, and several models have been developed that analytically represent the experimental findings of how concrete behaves under various stress states. The Drucker-Prager Yield Criterion (Drucker & Prager, 1952) is a popular model for representing concrete failure, as it is able to capture concrete's strength in compression, it's weakness in tension, and concrete's behavior under bi-axial and tri-axial stress conditions. A graph with examples of the failure envelope is shown in Figure 10. Therefore, a goal of the experiment was to write a topology optimization algorithm that could contain the internal stresses within a Drucker-Prager failure envelop as a constraint. The Drucker-Prager stress constraints in 2D are described succinctly by Bruggi and Duysinx as:

$$\sigma^{\mathrm{eq}} = \frac{s+1}{2s}\sqrt{3J_{2D}} + \frac{s-1}{2s}J_1 \leq \sigma_{Lt}$$

Where $\sigma^{eq}$ is the allowable stress states, $\sigma_{Lt}$ is the tensile limit of the material, $s$ is the ratio between the compressive limit and tensile limit of the system, $J_1$ is the first stress invariant, and $J_2$ is the second deviatoric stress invariant, such that:

$$J_1 = \sigma_{11} + \sigma_{22},$$
$$3J_{2D} = \sigma_{11}^2 + \sigma_{22}^2 - \sigma_{11}\sigma_{22} + 3\sigma_{12}^2$$

An algorithm implementing a stress-constrained topology optimization algorithm that utilizes the Drucker-Prager failure envelope was developed by Bruggi and Duysinx (Bruggi & Duysinx, 2012). In this paper, the volume of the system is minimized such that all of the stresses are maintained within the failure envelope.

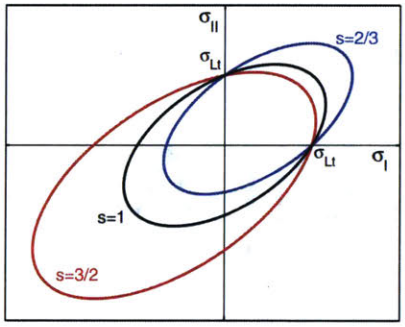


*Figure 10: Visualization of Drucker-Prager yield criterion, showing three different ratios of compressive strength to tensile strength. Borrowed from Bruggi and Duysinx (Bruggi & Duysinx, Topology optimization for minimum weight with compliance and stress constraints, 2012)*

A drawback of stress-based topology optimization algorithms is that they are extremely demanding on computational time. Each iteration tends to take much longer than a compliance-based optimizer. Compliance is a global phenomenon which only requires one calculation to check. By contrast, a stress-based optimizer seeks to evaluate the stresses at each element of the entire system, which involves as many checks as there are elements in the system. Unsurprisingly, this can become extraordinarily time-consuming. A way to alleviate long computational time is by utilizing a P-norm function, which seeks to estimate the maximum global stress in the system (Le, Norato, Bruns, Ha, & Tortorelli, 2010). The formulation of the P-norm is shown below:

$$\sigma_{PN} = \left( \sum_{e=1}^{N} v_e \sigma_e^P \right)^{1/P}$$

Where $v_n$ is the volume of an element, $\sigma_e$ is the stress in the element, and P is a variable chose by the designer.

Upon inspection, it can be seen that by exponentiating all the stresses, the larger values in the formulation dominate the equation, and the output is fairly close to the largest number in the set. In this way, the p-norm allows designers to extract an estimate of the largest number in a single formulation that is differentiable, thus making it ideal for computationally intensive optimization problems. Differentiability is useful because the gradients of the objective functions and the constraints can be used to guide the optimizations, thus requiring less time and generating better results.

By implementing the p-norm combined with the Drucker-Prager stress criterion, a topology optimization algorithm was achieved that could efficiently maintain internal stresses below the values at which concrete would fracture, and do so in a time-effective manner. The optimization, which shall be referred to as a stress-based optimizer, is formalized as:

$$\begin{aligned}
\underset{\phi}{\text{minimize}} \quad & f = \sum_{e \in \Omega} \rho^e v^e \\
\text{subject to} \quad & \mathbf{K}(\rho^e)\mathbf{d} - \mathbf{F} = \mathbf{0} \\
& \sigma_{min} \leq \left( \left( \sum_{e \in \Omega} v^e \sigma_{DP}^e \right)^P \right)^{1/P} \leq \sigma_{max} \\
& \phi_{min} \leq \phi_i \leq \phi_{max} \quad \forall\, i \in \Omega
\end{aligned}$$

Here, the objective function is minimizing the volume of the structure, as noted in the first line of the formulation. The second, third, and fourth lines are again the constraints of the problem. The only constraint that differs from the compliance-based optimizer is the third line, which shows the p-norm function constraining the estimated maximum stress within the boundaries chosen by the designer.

It should be noted that the P-norm is known to have problematic effects in its implementation. Since the value of P has no real-world correlate, it is chosen case-by-case to the discretion of the designer, which can lead to differing and potentially problematic results (Le, Norato, Bruns, Ha, & Tortorelli, 2010).

For the case of the concrete design, the p-norm is particularly problematic, because the optimizer is attempting to constrain the Drucker-Prager criterion to two different values, a positive tensile capacity and a negative compressive strength. It was found during the design process that only even values of p were conducive with the p-norm formulation, such as P = 4, 6, 8, and so on. This is because odd values could allow for negative numbers within the radical, which would produce imaginary solutions and crash the algorithm. Since all stresses were taken to an even integer, any negative stress states would be understood as positive after being formulated through the p-norm function. This phenomenon created the potential for inaccurate results from the stress-based optimizer, which relies on differentiating between "positive" tensile stresses and "negative" compressive states.

However, in the load case chosen for the herein presented experiments, this complication was found to be irrelevant. In the design load case, tension forces dominate the system, which means the positive values will be correlated with the maximum result from the p-norm formulation. Additionally, the tensile forces are the most important for the concrete optimizer, as they control the ultimate capacity of the system. Because the p-norm focused on constraining tensile values within the structural system, the tensile values dominated the particular load case, and the tensile forces are what limited the specific construction material, this was deemed an acceptable use-case for the p-norm formulation.

It should also be noted that the maximum and minimum stress levels were output at each iteration of the optimization. These outputs were monitored continuously, and stayed within the bounds placed upon the system by the designer.

In conclusion, a materially specific topology optimization code was written for the design of plain concrete structures. The optimizer could constrain forces within a Drucker-Prager failure envelope to account for concrete's anisotropic behavior, and it used a p-norm formulation to reduce computation time. This algorithm was used to design optimized concrete structures, as explained in the following section.

**Structural design:**

After the topology optimization algorithm had been written, it was necessary to use the algorithm to design structural elements that would be built. This experiment was conducted to compare the efficacy of two different topology optimization algorithms in the design of plain

concrete structures. In order to select a load case that would highlight the difference in the treatment of tensile stresses, which is the vital consideration for plain concrete, the Hammerhead Pier benchmark problem was chosen. The final load case is visualized below:

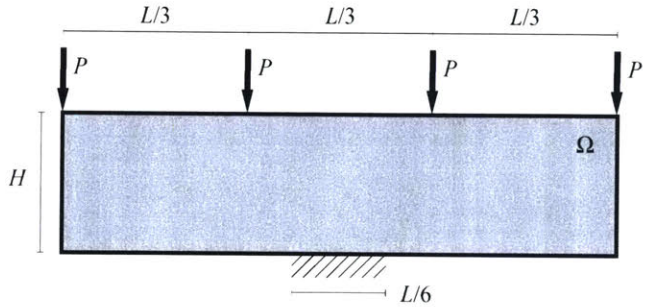


*Figure 11: Diagram of load case for optimized concrete, where L = 36" and P = 500 lbs*

Experimenters generated 5 designs based on this load case, which are outlined in Table 1, and further explained in the following sections.

| Name | Optimization | Volume[1] | Visualization |
|---|---|---|---|
| Compliance | compliance-based | 50% |  |
| High Tension | stress-based $f_t' = 8\sqrt{f_c'}$ | 49% | 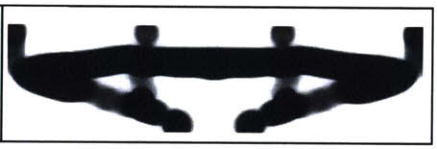 |
| Low Tension | stress-based $f_t' = 6\sqrt{f_c'}$ | 56% |  |
| Reinforced[2] | compliance-based | 50% |  |
| Control | none | 100% |  |

*Table 1: Algorithms used for concrete specimen design, with outputs shown*

[1] Volume calculated as $\frac{\Sigma(v^e \rho^e)}{A_t}$, whereе total area of the design space (324 sq. inches)

[2] The Reinforced design had a single no. 3 piece of rebar along its tension cord, which was bent in the MIT Blacksmithing lab to follow the beam's tension cord. The steel is designated by the red line in the figure

It was decided that five different designs would be tested for these experiments, and three of each design was fabricated for the tests. Thus, a total of 15 beams were fabricated.

The first would be the Compliance design, which was generated by a compliance-based optimization programmed to minimize the compliance of the beam while maintaining the volume at 50% of the available design space.

The second two designs were generated using the stress-based optimizer, which maintained internal stresses within the Drucker-Prager failure envelope, and reduced the volume as much as possible within those bounds. A 5,000 psi concrete was selected for the experiments, and therefore 5,000 psi was specified as the maximum compressive stress for the Drucker-Prager formulation. Because it was not possible to accurately predict the tensile capacity of the concrete before the curing process had finished, the designs differed in what each assumed the tensile capacity of the concrete to be. The High Tension design assumed a tensile capacity of $8\sqrt{f'c}$ for the concrete, or 565.7 psi, while the Low Tension design assumed a tensile capacity of $6\sqrt{f'c}$, or 424.3 psi. These are the bounds within which concrete is predicted to fail in tension (Nilson, Darwin, & Dolan, 2008). It was found that even this small change in the assumptions of the concrete strength could generate significant differences in structural design.

A fourth design was an entirely experimental Reinforced design. A Compliance design was generated, and a piece of number 3 rebar was placed into the tension chord, as can be seen in Figure 12. such that it would have ample tensile capacity. This design was made to test what the capacity of a reinforced concrete member might be, even though the steel cross-sectional area was not designed strictly with a topology optimization algorithm.

Finally, the fifth design was a control beam, which was a solid rectangle of concrete, or 100% of the design space volume.

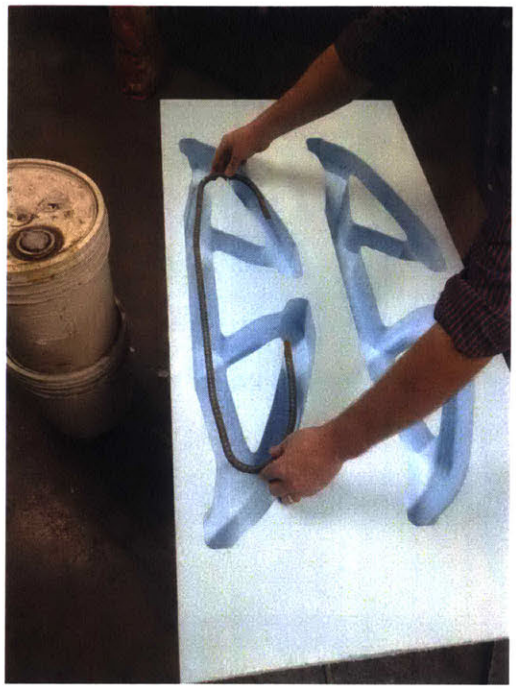

*Figure 12: Bent rebar used for Reinforced beam design*

The choice of what load cases and design domain to use depended on the constraints of the equipment available to the experimenters. To fabricate the specimens, concrete molds would be milled from Styrofoam which came in 24" x 96" sheets. This helped define a length-to-depth ratio of 4:1. In order to provide adequate thickness of Styrofoam around the edges of the molds, a 36"x9" dimension was chosen. The beams were designed with a 3" depth to ensure stability. Four point loads of 500 lbs were administered to the system, for a total of 2,000 lbs. It was assumed that the base support was a clamped connection capable of resisting moment.

In addition to the sizes of the design domain, a minimum length scale of 2" was selected to ensure manufacturability of the concrete. Concrete is an extremely brittle material, and when elements get small, they can fracture easily. It was essential that the concrete remain thick enough that it could be removed from the molds. For this reason, the minimum length scale was enforced using the Heaviside projection method. 2" was chosen because this is the minimum scale specified by the concrete used in the experiment.

Many different parameters of the optimization script had to be tested before a design was selected. All were carefully selected to yield the best designs possible. For the stress-based optimization, the value of P was set at 6, and the continuation method was used such that the values of other key variables changed after a set number of iterations. The value of $\eta$ grew from 1 to 9 at

a rate of .5 every 25 iterations, while β increased from 0 to 50 by rate of 1 every 25 iterations. When β reached a value of 50 and ηreached a value of 9, the optimization continued for 200 iterations. These values were used for both the High Tension and Low Tension designs.

For the compliance-based optimization, η increased from 1 to 5 at a rate of 1 every 50 iterations. β stayed at a value of 0 until eta reached its maximum value, at which point it increased to 50 at a non-linear rate, but changing every 50 iterations. Once η reached a value of 5 and β reached a value of 50, the optimizer ran 200 more iterations, then terminated.

Because the Compliance, High Tension, and Low Tension designs were the most rigorously produced, they warrant more thorough discussion. Their optimization outputs are enlarged in Figure 13:

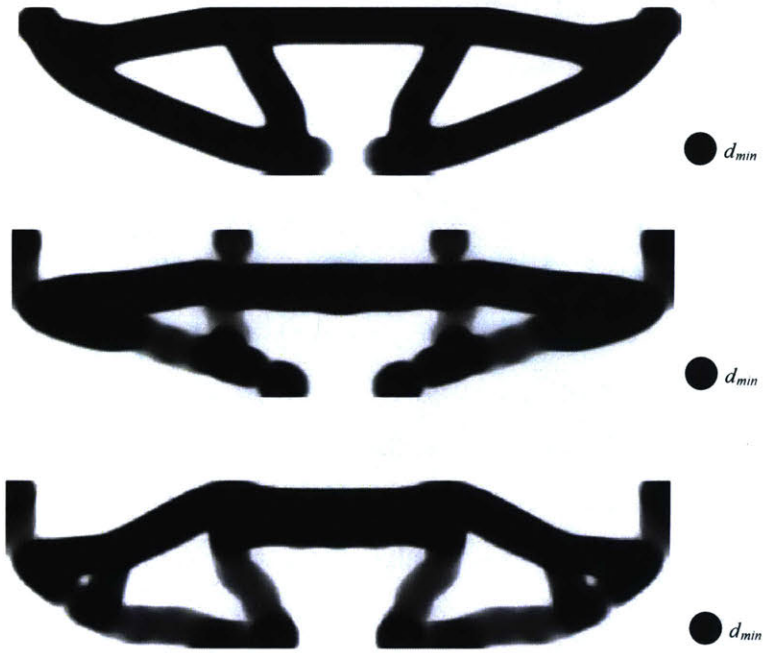


*Figure 13: Outputs for Compliance design (top), High Tension design (middle), and Low Tension design (bottom)*

It can be seen that the Compliance design has one compression strut originating from each point load, carrying forces to the clamp connection at the base of the beam, and a single tension element running along the top of the design domain. It appears that the dimensions of every element is roughly equal, except perhaps where they meet. Over the entirety of the design, the 2" minimum length scale is respected.

The High Tension design overall is similar to the Compliance design. By comparison, though, the High Tension beam has increased the cross-sectional area of the tension cord slightly, but also moved it closer to the base of the system. This may have been done in an effort to save material, as minimizing the volume is the objective function for this optimizer.

The Low Tension beam, on the other hand, increases the size of its tension cord dramatically, which bifurcates at either end to lend further support integrity to the specimen. This is because this material is even weaker in tension, and therefore more of it is needed to resist the forces put into the system.

It should be noted that the stress-based optimizer was not able to achieve a crisp 0/1 output in either the Low Tension or High Tension designs. Rather, the design calls for intermediate densities throughout the domain, particularly in the compression struts. It is believed that this is because of the large minimum feature length enforced in the optimization parameters, which forced the compressive struts to be highly over-engineered for the forces they were taking. With a 2"x3" minimum size, a compressive element could handle 30,000 lbs of direct compression force, but only 2,000 lbs total was being put into the system in total. For this reason, it was difficult to tune the optimizer such that it would respect the minimum feature length in the compressive areas.

To demonstrate the minimum feature length as the cause of the gradient outputs, the optimization script was run with a smaller length scale requirement of 1" instead of 2". The output is shown in Figure 14, and can be seen to be much closer to a 0-1 result, which suggests that the large length scale caused the gradient output.


*Figure 14: Stress-based output of High Tension design with 1" minimum length scale*

In order to address the non-binary output, experimenters rounded the output values of the densities in these areas, such that material would be placed wherever $\rho > 1/2$. Rounding yielded the models seen in Figure 15, which were used as the final designs for the fabrication process of the experiment:

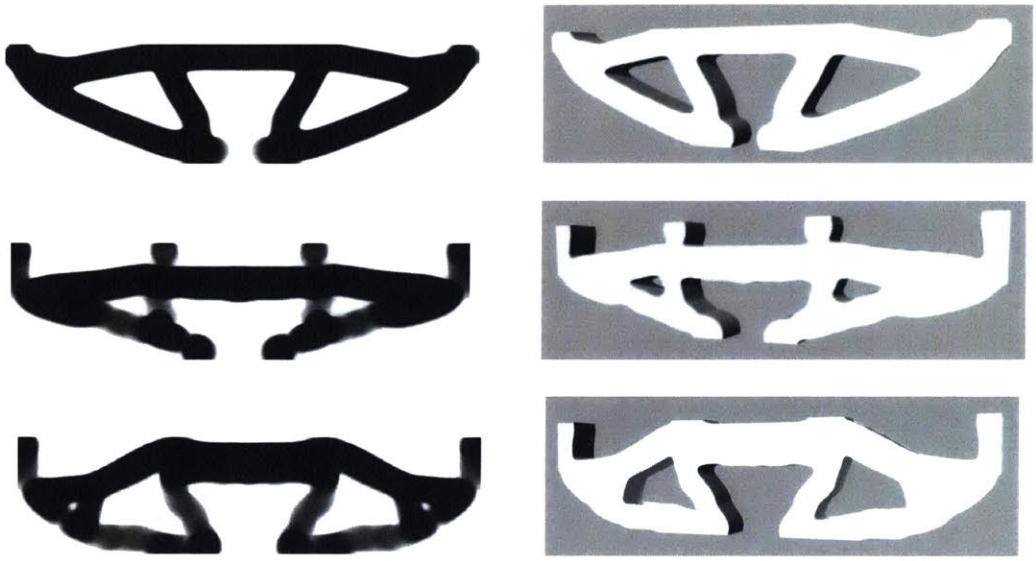

*Figure 15: Renderings of optimization outputs (left) and 3D designs used for concrete beam fabrication (right)*

**Fabrication**

After the concrete specimen designs had been finalized, it was necessary to fabricate the molds for the concrete.

Many different methods were considered for how to make the concrete molds, including building formwork from laser cut polygonal pieces, using fabric-formed techniques, and 3D printing the molds using PLA. Ultimately, it was decided that milling the formworks from Styrofoam blocks as a subtractive manufacturing method would be the most cost-effective and time-efficient process to fabricate accurate molds for the concrete.

To fabricate the molds, two sheets of 2" thick Styrofoam were bonded together using a polyurethane-based adhesive to create large pieces of 96"x24"x4" Styrofoam. The faces of the Styrofoam that would be bonded were lightly sanded to roughen the surface, then coated sparsely with water, then covered with a thin layer of adhesive. The sheets were then placed on top of each other, and weighted upon one another using a vacuum table exerting 5 psi, for a total of approximately 11,500 lbs. The adhesive was allowed to cure for 4 hours. Milling was done with a ONSRUD 3-axis mill using a ½" diameter bit, using MasterCam software for generating the toolpath. Images of the bonding process and the resulting formworks are shown in Figure 16. Cutting a single mold took approximately 4 minutes. 3 samples of each design were cut, resulting in a total of 15 cuts.

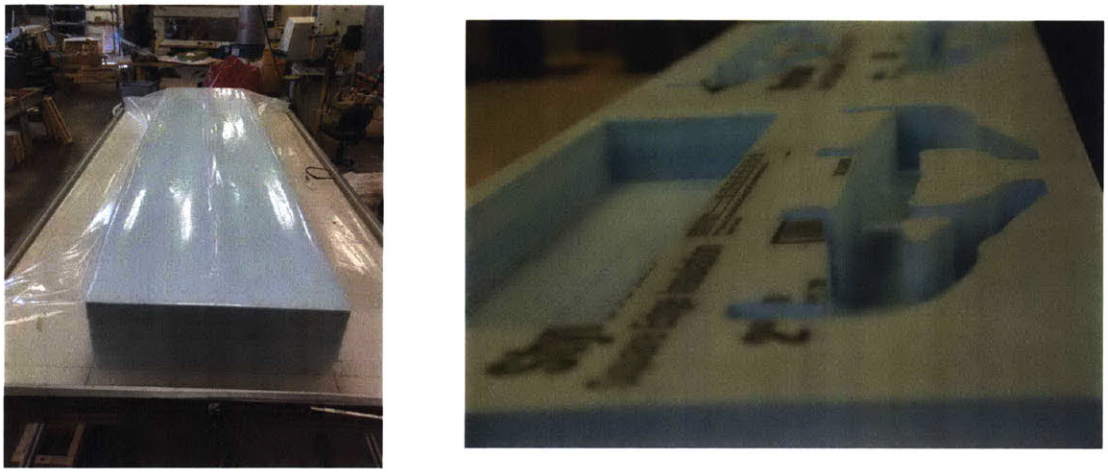

*Figure 16: Bonding Styrofoam loaded with vacuum table for effective cure (left), and resulting molds from milling machine (right)*

After the molds were cut, they were lined with a generous layer of white petroleum jelly to act as a release agent. Lined molds were filled with a 5,000 psi Quikrete ready-mix concrete with a maximum aggregate size of ½" diameter. Figure 17 shows the molds prepared for concrete, and mid-way through the filling process. Slump tests were administered following ASTM standards (Standard Test Method for Slump of Hydraulic-Cement Concrete, 2015), and yielded a slump of approximately 1" for each batch of concrete, which was deemed acceptable. Molds were filled, and placed on a shake table for adequate time to allow concrete to settle and remove air pockets within the concrete.

*Figure 17: Molds with release agent, and filled with concrete*

After the concrete was placed in the molds, it was covered with plastic liner and given an initial cure of 7 days. To ensure a humid environment, every day the liner was removed, a fresh

layer of water was sprayed onto the concrete, and the liner was replaced. After the initial cure, concrete was removed from its molds and placed into a plain water bath for over 28 days, as illustrated in Figure 18.

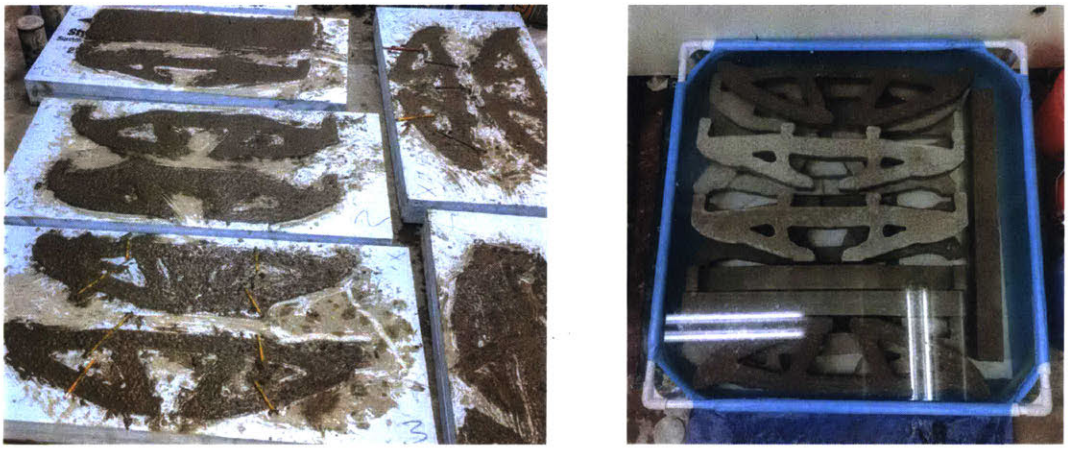

*Figure 18: Concrete curing in molds*

Concrete was also collected into 4" diameter cylinders to test for strength after the concrete had cured. Four batches of concrete were mixed over the course of the experiments, and not every batch was large enough to afford enough concrete for use in cylinders. 6 cylinders were taken from the first batch of concrete, 2 from batch 2, 6 from batch 3, and 3 were collected from batch 4. Examples of these cylinders are shown in Figure 19; they were tested for compressive and tensile capacity after they had fully cured.

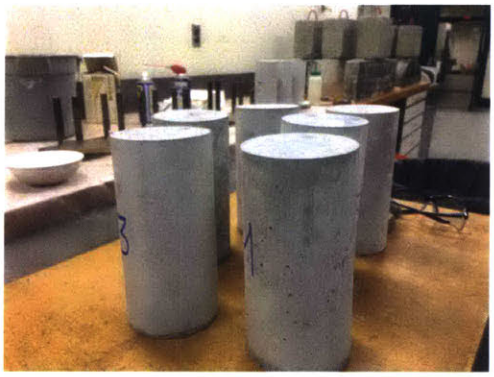

*Figure 19: Cylinders collected from concrete batches*

After the concrete had cured, the release agent was removed from the samples using an angle grinder with metal brush head, and plaster caps were placed on the concrete wherever the

concrete would be in contact with the testing apparatus. Steel plates of ¼ inch thickness were adhered to the bottom of the concrete with a high-strength 3,500 psi epoxy to simulate the pin connection used in the optimization support conditions. A High Tension beam prepared thusly for testing can be seen in Figure 20.

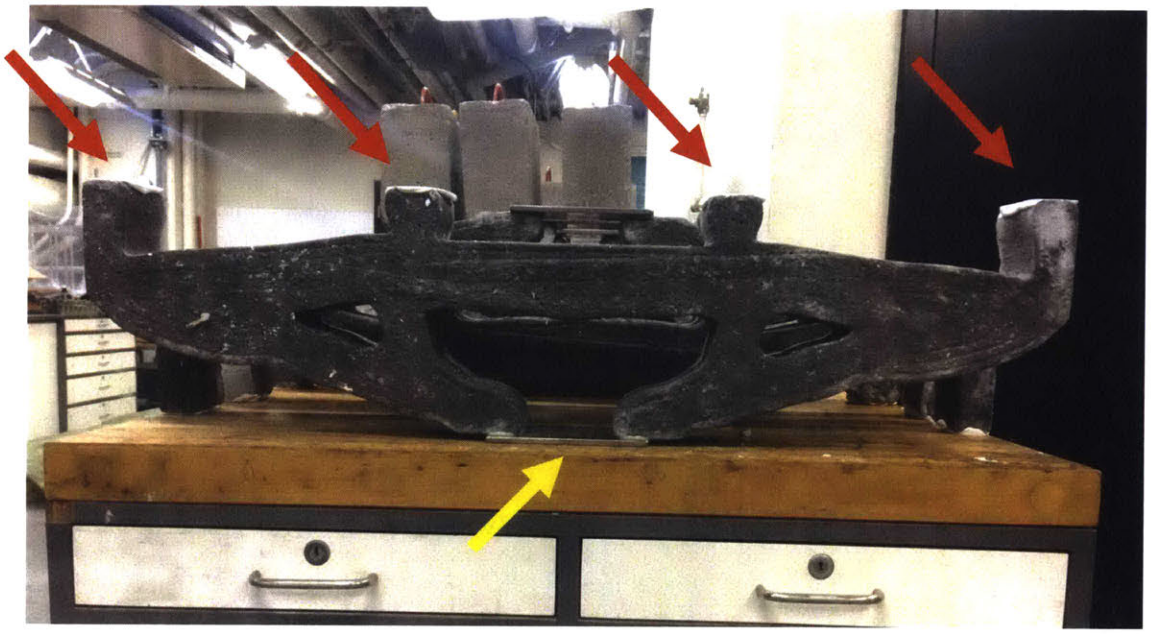

*Figure 20: Beam prepared for testing, with plaster caps marked with red arrows and the epoxied steel plate designated with the yellow arrow*

**Testing**

In addition to fabricating the concrete molds, a testing apparatus was also fabricated that would deliver the unconventional load case into the concrete specimen.

It was necessary to ensure that the apparatus would not deflect significantly during testing, and that loads would be administered evenly throughout the course of the experiment, even if there were asymmetric settlements in the system. Square steel HSS tubes of ¼" thickness were used to administer the loads such that they would deflect less than $1/100^{th}$ of an inch at a load of 50,000 lbs. By balancing a tube at its midpoint on a cylindrical steel rod, it can be assured that the forces acting on either end of the tube are equal. Using this principle, two 12" long tubes were balanced on their midpoints, and spaced 12" apart end-to-end, so that their endpoints were located where the forces needed to be delivered. Every point of contact in the system rested on steel rods sitting within grooved steel plates to simulate point loads as accurately as possible, and those grooved

plates were welded to the steel tubes to ensure stability. The fabrication process, and the resulting hardware, can be seen in Figure 21.

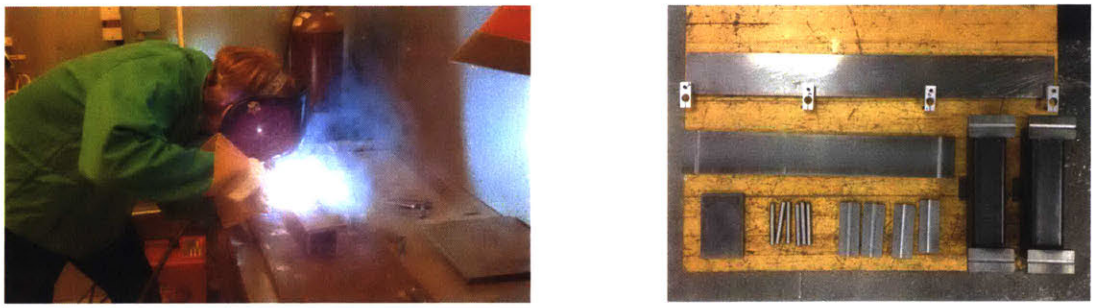

*Figure 21: Fabrication of testing apparatus, and finalized testing apparatus*

To evaluate the accuracy of the computational models developed for these designs, it was necessary to measure the deflections of the concrete specimens during loading. In particular, because many topology optimization algorithms use the compliance of the system as their objective functions, it was desirable to measure the deflections at each of the point forces in the system. To achieve this goal, 4 linear variable differential transducers (LVDTs) were affixed to the concrete specimens, such that they were securely fixed to a rigid steel plate at the top of the specimen, and rested on steel plates beneath the specimen, where the forces were delivered. As the plates moved due to deflections of the concrete specimens, the LVDTs would track these displacements, and record them in a data set that was collected and interpreted after the experiments. The CAD rendering of a beam in the testing apparatus, and a photo of the built models prepared in the testing apparatus, can be seen side-by-side in Figure 22.

*Figure 22: CAD model of beam in testing apparatus, and photo of beam in testing apparatus*

Each concrete beam was placed within the testing apparatus mounted on a Baldwin Universal Testing Machine (UTM), as shown in Figure 23. Force was applied with a displacement-controlled method, and both the forces and the deflections were recorded during the tests. Although all beams were designed for elastic behavior, samples were tested until failure so data could be collected both at the design load, as well as outside the limits of the optimization. The results are discussed in the following section.

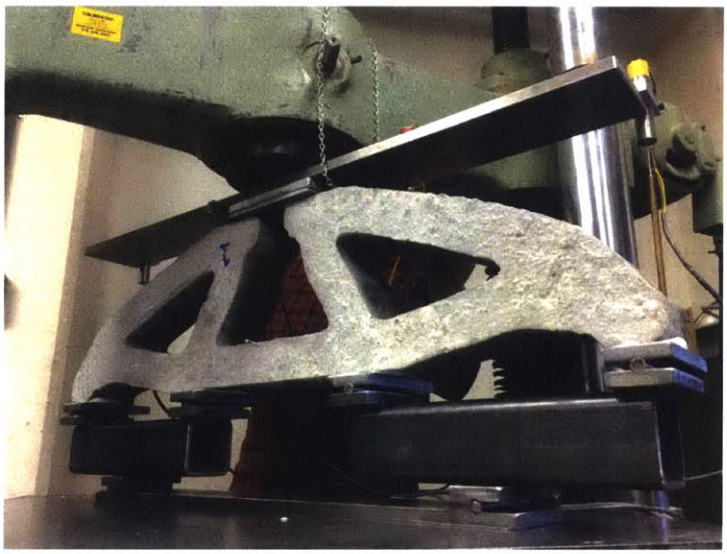

*Figure 23: compliance beam in testing apparatus*

Cylinders tested for compressive capacity were capped, centered on the testing apparatus, and brought to failure. Loads were recorded over the course of the test, and two extensometers were attached to each compression cylinder to derive the elastic modulus of the concrete.

Cylinders tested for tensile capacity were also tested in the Baldwin UTM using the Brazilian split-cylinder method (C 496/C 496M – 04, 2004). Concrete cylinders were placed on their sides with a $1/8^{th}$ inch thick strip of rubber on top of and beneath the concrete. The cylinders were centered beneath the plate of the UTM, and loaded until failure.

# Results

The results of these experiments were surprising, and required careful scrutiny to be understood. The concrete strength was found to be 6,810.2 psi in compression and about 642.28 psi in tension, with an elastic modulus of 3,690.67 ksi. The strengths were much higher than had

been predicted. The elastic modulus had been predicted to be 4030 ksi, so the derived value was significantly lower. The results from the cylinder tests can be seen in Tables 2 and 3. Both of these values greatly exceeded the strengths used in the optimization's Drucker-Prager failure boundaries, as they were much higher than expected.

| Batch | Sample | Max Load (lbs) | Tensile Capacity (psi) | Notes | Batch Average | Total Average |
|---|---|---|---|---|---|---|
| **1** | 1 | 39847.957 | 792.7499161 | unsatisfactory rubber thickness used | **663.4226684** | **642.2779992** |
| | 2 | 34496.816 | 686.2923484 | | | |
| | 3 | 32197.705 | 640.5529884 | | | stdev = 45.35 |
| **2** | 1 | 37152.75 | 739.1304765 | poor sample of concrete | **0** | |
| | 2 | 23447.828 | 466.4797164 | unsatifactory Break | | |
| **3** | 1 | 30608.855 | 608.943822 | | **608.943822** | |
| | 2 | 28430.926 | 565.6153012 | Poor concrete cylinder sample | | |
| | 3 | 26984.582 | 536.8412016 | Broke orthagonal to desired splitting plane | | |
| **4** | 1 | 29827.898 | 593.4071761 | | **654.4675072** | |
| | 2 | 33035.887 | 657.2280894 | | | |
| | 3 | 35827.59 | 712.7672559 | | | |

*Table 2: Results from concrete cylinder tensile tests (Above). Samples with unsatisfactory results are marked in red, and their data were eliminated from the results of the experiment*

| Batch | Sample | Max Load (kips) | Compression Capacity (psi) | Batch Average (psi) | Elastic Modulus (ksi) | Average Elastic Modulus (ksi) |
|---|---|---|---|---|---|---|
| 1 | 1 | -85.34 | 6791.26 | 6793.113931 | 3892.19 | 3806.26 |
| | 2 | -83.3 | 6628.8 | | 3753.05 | |
| | 3 | -87.45 | 6959.28 | | 3773.54 | |
| | | | | | | |
| 3 | 1 | -86.71 | 6900.7 | 6827.242931 | 3442.07 | 3575.09 |
| | 2[1] | -78.07 | 6212.72 | | 3311.84 | |
| | 3 | -84.87 | 6753.79 | | 3708.11 | |

*Table 3: Results of cylinder compression tests (above). The sample marked in red was deemed unsatisfactory, and its data were eliminated from the final analysis*

| Design | Sample | Concrete Mix | Max Load (lbs) | Average (lbs) |
|---|---|---|---|---|
| Compliance | 1 | 1 | 6,389.048 | 5,095.305 |
| | 2 | 1 | 5,298.399 | |
| volume = 50% | 3 | 3 | 3,598.468 | |
| | | | | |
| High Tension | 1 | 1 | 3,230.43 | 3,363.207867 |
| | 2 | 2 | 3,907.0361 | |
| volume = 51% | 3 | 1 | 2,952.1575 | |
| | | | | |
| Low Tension | 1 | 4 | 4,557.835 | 4,819.650533 |
| | 2 | 2 | 4,933.727 | |
| volume = 56% | 3 | 2 | 4,967.3896 | |
| | | | | |
| Control | 1 | 4 | 24,799.918 | 25,257.721 |
| | 2 | 4 | 27283.05 | |
| volume = 100% | 3 | 2 | 23690.195 | |
| | | | | |
| Reinforced | 1 | 3 | 19,532.938 | 17,769.0485 |
| | 2 | 3 | 17,907.062 | |
| volume = 50% | 3 | 3 | 15,867.1455 | |

*Table 4: Results from tests of concrete beams (above)*

[1] Sample 2 from batch 3 of concrete was extremely porous, its results were eliminated from the analysis

### Control, Reinforced, and Low Tension Results

First, it should be noted that the reinforced beams did not fail due to steel or concrete yield. Rather, the epoxy at the base of these concrete specimens did not bond thoroughly with the steel plates, and local shear force caused the epoxy to de-laminate before the specimen itself could fail. Thus, it is evident that the pinned connection detail was not adequately established in the fabricated specimen. This is likely due to the fact that the steel was not roughened before the epoxy was applied, and the steel's smooth surface did not provide a sufficient surface to which the epoxy could adhere. The reinforced beams de-bonded at 17,769 on average.

The control beams were extremely strong, failing at an average strength of 25,257.72 lbs. Each of them failed in shear. The results were informative for future experiments, but will not be discussed further in this thesis.

Due to time and experimental constraints, results from the Low Tension design were not thoroughly investigated. Particularly, this is because the volume of the Low Tension beam was significantly different than the Compliance beam of or the High Tension beam, and it was decided that direct comparison with the other designs was inaccurate.

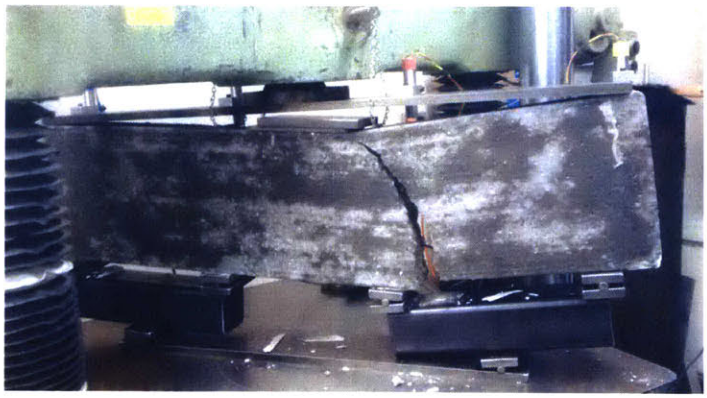

### Compliance and High Tension Results Comparison

The designs that will be considered with the greatest detail are the Compliance designs, and the High Tension designs. These two designs offer excellent insight into the efficacy of the topology optimization algorithms, because they had nearly identical volumes, and two of the three samples were made from the same concrete mix. The rounded High Tension design had a volume of 51% of the design space, while the compliance design had a volume of 50%. Thus, there is a

high degree of experimental control between these two designs; they differ only in which algorithm was used to design them.

The High Tension design was able to withstand an average load of 3,363.2 lbs. Recall that the purpose of this algorithm was to minimize the volume of the concrete while maintaining internal forces within the Drucker-Prager failure envelope. To this end, the algorithm was successful in achieving, and even surpassing, the design load of 2,000 lbs. One explanation for the over-performance of these beams is that the concrete was stronger than had been expected. The compressive strength of the concrete was 6,810.2 psi, which far exceeded the expected value of 5,000 psi, around which the beams were designed.

The Compliance beam, by comparison, achieved an average load of 5,096.3 lbs, which is much higher than the High Tension design. This is a surprising result, as the Compliance design was made with an optimization algorithm that had not been programmed to design around concrete's anisotropic behavior. Without being programmed to account for the building material's behavior, it was expected that this design would perform poorly. Rather, the Compliance design failed at a load almost 50% higher than the concrete-specific algorithm.

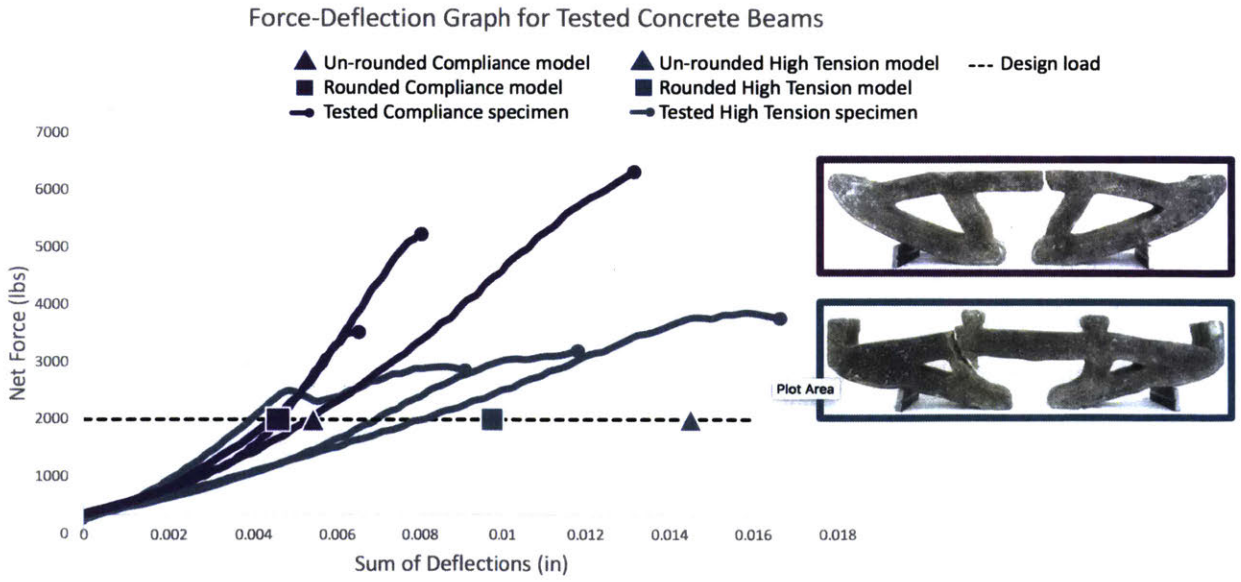


*Table 5: Stress-Strain relation of Compliance and High Tension samples*

The graph in Table 3 shows the stress-strain relation of the Compliance design beam and the High Tension design beam. The Sum of Deflections was calculated by adding the deflection

readings from all four LVDTs at any given time, and the net force is the total force going into the system. Thus, the magnitude of each point load is on-fourth of the Net Force.

The graph also shows the calculated Net Deflections for the computational models at the design load before and after the designs were rounded. In other words, the un-rounded optimization outputs were analyzed in Matlab for deflection at 2,000 lbs, then the rounded computational models were analyzed in ABAQUS for deflection at 2,000 lbs, and finally the physical beams were tested and their behavior was recorded until failure.

It should be noted that the LVDT outputs required significant adjustment to produce meaningful outputs. It was often the case that one LVDT reading was inaccurate, for example showing an upwards deflection at the point load. When this occurred, the erratic measurement data were eliminated, and the corresponding measurement was doubled. That is to say, for example, if the left-most outer point load data were deemed unsatisfactory, they were eliminated, and the right-most data were doubled to compensate. The LVDT readings were also re-zeroed after the system had been loaded with a small force to account for the seating of the measurement equipment.

It can be seen that the rounded models were stiffer than the unrounded models. This effect was quite small for the Compliance design, which shows that the rounding had little effect on the specimen. However, the shift was dramatic for the High Tension design. This is not overly surprising, as significant material was added to the system after it had been rounded.

Surprisingly, the tested High Tension beams were even stiffer than the rounded computational model had predicted, despite having a lower elastic modulus. This result may have been due to measurement error in the LVDTs, or due to lateral deflections at the point loads being misinterpreted by the equipment.

Of particular interest, of course, is the difference in maximum load. It was not expected that the Compliance design, which had not been programmed to account for the fabrication material, would be stronger than the High Tension design, which had been made specifically for optimizing concrete. It is likely that this discrepancy is due to the rounding that had been done on the High Tension beam during the design phase of the experiment. The evidence for this lies in the failure modes exhibited by the beams.

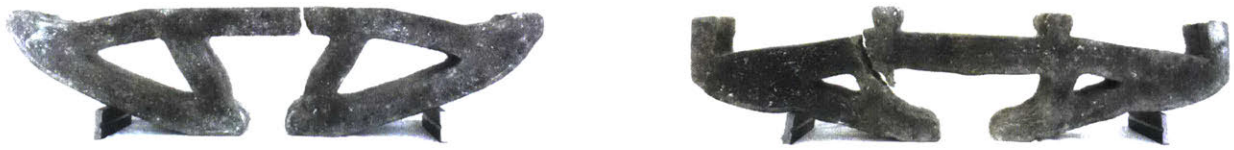

*Figure 24: Typical Compliance and High Tension beam after testing*

The Compliance beams failed in their tension chords orthogonal to the flow of forces, suggesting a tensile failure. By contrast, the High Tension beams failed along an angled path just outside of one of the interior point loads, which typically signifies a shear failure.

It is likely that the difference in failure modes explains the difference in maximum load capacities of the two designs, as the tensile capacity of concrete is higher than the shear capacity ($8\sqrt{f'c}$ vs $2.5\sqrt{f'c}$).

**Computational Analysis**

It should have been expected that the High Tension design would be able to account for the difference in failure modes, as this weakness should have been capture by the Drucker-Prager failure envelope and avoided by the optimizer. However, it is likely that the difference in failure modes was not in the optimizer's original design. Rather, it likely arose after the optimization outputs were rounded in an effort to ensure manufacturability.

A stress map showing the magnitude of the first principle stresses was generated using Matlab for the "pre-rounded" designs, shown in Figure 25. In other words, the gradient outputs from the optimizer were used for a FEM analysis, and the largest principle stresses were mapped onto the structure, to show where the stress concentrations lay.

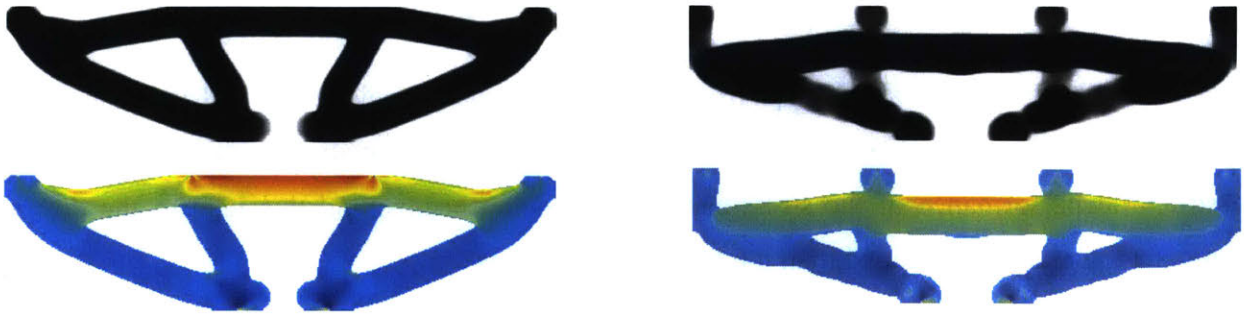

*Figure 25: Optimization outputs before rounding (above) compared to stress concentration maps of un-rounded specimens (below). Compliance designs are shown on the left, while High Tension designs are shown on the right*

It can be seen that the stress concentrations in both of these models lie in the center of the tension cord. This is unsurprising, as this load case causes large tensile capacities to develop along the top of the design space due to the long moment arm from the outer point loads.

A FEM analysis was also run in ABAQUS on the rounded models at the design loads, to examine whether or not the stress concentrations were affected by changing the structural design.

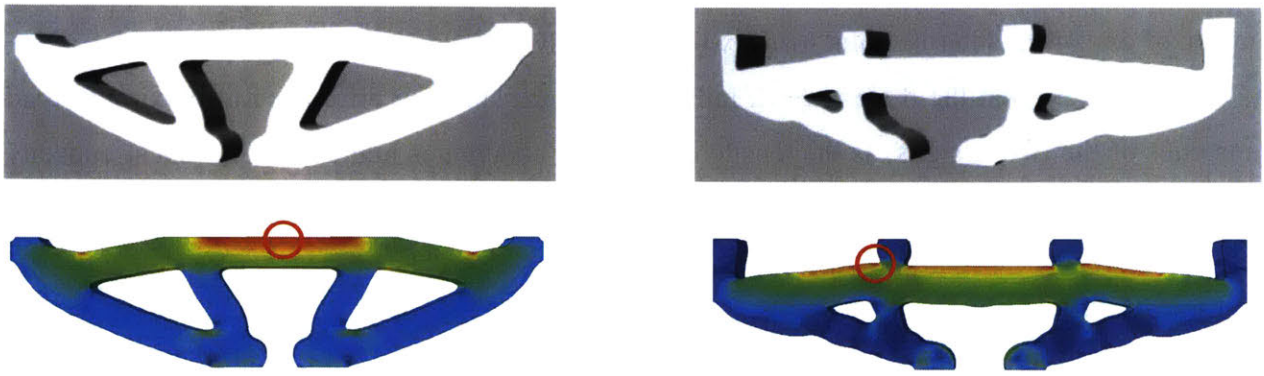

*Figure 26: Optimization outputs after rounding (above) compared to stress concentration maps of rounded specimens (below). Compliance designs are shown on the left, while High Tension designs are shown on the right. Locations of maximum stresses noted with red circles.*

As can be seen in Figure 26, the Compliance design stress concentrations are almost unchanged from the un-rounded model. This is not surprising, as the model itself was almost unchanged from the original output to the fabricated element.

In contrast, the High Tension model's FEM analysis yields a significantly different result. High stress values are distributed across the top of the beam, and notably, the location of maximum stress lies just outside of the inner point load. This is the exact location of the shear failure exhibited by the High Tension specimens.

Due to the change in stress maps from the computational models before and after rounding, it is reasonable to conclude that rounding the results of the optimization algorithms fatally hindered the structural performance of the stress-based optimization beams, and this lead to the design failing at a lower maximum load than the Compliance beams.

# Conclusion

This thesis aimed at designing, fabricating, and testing concrete beams that were designed with topology optimization algorithms. Two different optimization algorithms were used to design concrete structures for the same load case, so the resulting designs could be compared with experimental testing. One optimizer assumed the fabrication material was isotropic and minimized the compliance of the system, while the other sought to find a minimum volume while maintaining the internal stresses of the system within a Drucker-Prager stress envelope. Designs were generated, fabricated, and tested, and the results were analyzed.

It was found that beams designed with the stress-based optimizer, which had been developed specifically for optimization of plain concrete structures, experimentally failed at lower loads than the compliance-based designs. It is believed that this surprising result is due to the rounding of the gradient output that was generated by the stress-based optimizer. FEM analysis showed that the stress concentration in the structure moved after the results were rounded, changing the failure mode from a tensile failure to a shear failure. It is believed that the alteration of the failure mode explains why the stress-based optimizer was outperformed by the compliance based optimizer. A key result of this experiment is a demonstration of the impact one can have when rounding the outputs of an optimization code. It may be assumed that adding material will always make a structure stronger, but these tests would suggest that one must add material in the right places to achieve truly optimized performance.

This experiment demonstrates the importance of building and testing physical specimens in the field of structural engineering. The discipline has benefitted greatly from years of computational experimentation, in which innumerable codes have been developed that each move the technology closer to something that can be applied to the design of civil-scale structures around the world. However, it is important to take the next steps in solving the problems of how to build these structures, and to ensure that they behave as we predicted. Recent advancements in digital fabrication tools, and accessibility of robust computational power, make the manufacturing of non-linear structures more accessible than it has ever been. It is crucial to leverage these tools with advanced structural optimization algorithms so more efficient structures can be built and tested. A wealth of knowledge awaits in this process of experimentation.

A crucial limitation of this work was a short timeline in which to do the experimentation, as there was only one semester to design, build, and test the concrete. Particularly since the concrete had to cure for 28 days, the design portion of the experiment had to happen quite quickly. However, the experience has highlighted opportunities for future researchers to improve upon these experiments.

Another critical limitation of these experiments is the use of plain concrete instead of reinforced concrete. There was immense value in simplifying the problem by excluding rebar, and solving the problems of how to optimize for a single material, as well as how to build the concrete formworks themselves. However, plain concrete is very rarely used in structural engineering applications, and the true impact of topology optimization technology for concrete design will come when reinforcing steel is introduced into the algorithm and fabricated specimens. It should be noted, though, that with the rise of 3D printing concrete (Asprone, Auricchio, Menna, & Mercuri, 2018), and other digital fabrication means for building non-traditional concrete elements, the assumptions of the use of concrete may be revisited, and this thorough understanding of fundamental concrete mechanics may prove more useful than ever.

Every computational tool makes assumptions that do not reflect physical world. Support conditions are considered to be perfect, inter-facial bonding is assumed not to slip, and materials are assumed to be defect free. Of course, when structures are built, the consequences of these assumptions are exposed, and structures rarely behave as they did in computational space. These experiments can demonstrate the numerous problems that can arise in this transition. It is only with caution, iteration, and perseverance that the experience of building and testing these optimized structures that the community can move towards advanced optimization tools being employed for the design of real-world civil-scale structures.

Not only can fabrication of optimized structures expose problems, but it can also expose opportunities. When building structures, new ideas become apparent, new tools become available, and new concepts expose themselves that had not been obvious in the computational space. It is the hope of the author that researchers will try to improve upon the experiments that were outlined in this paper, and in doing so produce better results with more applications than had been available at the conclusion of this particular project. Civil engineering deserves its digital revolution, but it will only happen if things get built.

# Bibliography


A. Liew, D. L. (2017). Design, fabrication and testing of a prototype, thin-vaulted, unreinforced concrete floor. *137, 323-335.*

Amir, O., & Shakour, E. (2018). Simultaneous shape and topology optimization of prestressed concrete beams. *Struct Multidisc Optim*, 57:1831–1843.

Amir, O., & Sigmund, O. (2013). Reinforcement layout design for concrete structures based on continuum damage and truss topology optimization. *47:157–174.*

Asprone, D., Auricchio, F., Menna, C., & Mercuri, V. (2018). 3D printing of reinforced concrete elements: Technology and design approach. *Construction and Building Materials*, 165, 218–231.

Bendsoe, M. P., & Kikuchi, N. (1988). Generating optimal topologies in structural design using a homogenization method. *Computer Methods in Applied Mechanics and Engineering* , 71(2): 197-224.

Bendsoe, M. P., & Sigmund, O. (2004). *Topology Optimization: Theory, Methods, and Applications.* Springer.

Bogomolny, M., & Amir, O. (2012). Conceptual design of reinforced concrete structures using topology optimization with elastoplastic material modeling. *90:1578–1597.*

Bruggi, M. (2016). A numerical method to generate optimal load paths in plain and reinforced concrete structures. *170 (2016) 26–36.*

Bruggi, M., & Duysinx, P. (2012). Topology optimization for minimum weight with compliance and stress constraints. *Struct Multidisc Optim* , 46:369–384.

C 496/C 496M – 04. (2004). *Standard Test Method for Splitting Tensile Strength of Cylindrical Concrete Specimens.*

Cavazzuti, M., Baldini, A., Bertocchi, E., Costi, D., Torricelli, E., & Moruzzi, P. (2011). High performance automotive chassis design: a topology optimization based approach. *44:45–56.*

Culver, R., Koerner, J., & Sarafian, J. (2016). Fabric Forms: The Robotic Positioning of Fabric Formwork. *Robotic Fabrication in Architecture, Art and Design*, (pp. pp 106-121).

Dapogny, C., Faure, A., Michailidis, G., Allaire, G., Couvelas, A., & Estevez, R. (2017). Geometric constraints for shape and topology optimization in architectural design. *59:933–965.*

Dombernowski, P., & Søndergaard, A. (2012). DESIGN, ANALYSIS AND REALISATION OF TOPOLOGY OPTIMIZED CONCRETE STRUCTURES. *JOURNAL OF THE INTERNATIONAL ASSOCIATION FOR SHELL AND SPATIAL STRUCTURES.*

Drucker, D., & Prager, W. (1952). Soil mechanics and plastic analysis or limit design. *Quarterly of Applied Mathematics, 10*, pp. 157-165.

Garbett, J., Darby, A., & Ibell, T. (2016). Optimised Beam Design Using Innovative Fabric-Formed Concrete. *13*(5).

Gaynor, A. T., & Guest, J. K. (2016). Topology optimization considering overhang constraints: Eliminating sacrificial support material in additive manufacturing through design. *Structural and Multidisciplinary Optimization*, Volume 53, Issue 1, pp 175–192.

Gaynor, A. T., Guest, J. K., & Moen, C. D. (2013). Reinforced Concrete Force Visualization and Design Using Bilinear Truss-Continuum Topology Optimization. *139(4): 607-618.*

Guest, .. K., Prévost, J. H., & Belytschko, T. (2004). Achieving minimum length scale in topology optimization using nodal design variables and projection functions. *International Journal for Numerical Methods in Engineering*, 61:238–254.

Hawkins, W., Orr, J., Shepherd, P., Ibell, T., & Bregulla, J. (2017). Thin-shell textile-reinforced concrete floors for sustainable buildings. International Association of Shell and Spatial Structures.

Januszkiewicz, K., & Banachowicz, M. (2017). Nonlinear Shaping Architecture Designed with Using Evolutionary Structural Optimization Tools. IOP Conference Series: Materials Science and Engineering.

Jipa, A., Bernhard, M., Dillenburger, B., & Aghaei-Meibodi, M. (2016). 3D Printed Stay-in-Place Formwork for Topologically Optimised Concrete Slabs. *TxA: Emerging Design and Technology*, (pp. p.96-107).

Le, C., Norato, J., Bruns, T., Ha, C., & Tortorelli, D. (2010). Stress-based topology optimization for continua. *Struct Multidisc Optim*, 41:605–620.

Liang, Q. Q., Xie, Y. M., & Steven, G. P. (2000). Topology Optimization of Strut-and-Tie Models in Reinforced Concrete Structures Using an Evolutionary Procedure. *97(2):322-332* .

Matteo Bruggi, P. D. (2012). Topology optimization for minimum weight with compliance and stress constraints. *46:369–384.*

Mehta, P. K., & Monteiro, P. J. (2004). *Concrete: Microstructure, Properties, and Materials.* McGraw Hill.

Nilson, A., Darwin, D., & Dolan, C. (2008). *Design of Concrete Structures.* McGraw Hill.

Orr, J., Darby, A., Ibell, T., & Evernden, M. C. (2011). Innovative reinforcement for fabric formed concrete structures. International Symposium on Fiber Reinforced Polymer Reinforcement for Concrete Structures.

Sasaki, M. (2007). *Morphogenesis of Flux Structure.* AA Publications.

Sigmund, O., & Bendsoe, M. (2004). *Topology Optimization-Theory, Methods and Applications.* Springer.

(2015). *Standard Test Method for Slump of Hydraulic-Cement Concrete.* ASTM International.

Svanberg, K. (1987). THE METHOD OF MOVING ASYMPTOTES-A NEW METHOD FOR STRUCTURAL OPTIMIZATION. *International Journal for Numerical Methods in Engineering*, VOL. 24, 359-373.

Van Mele T., M. E. (2018). A prototype of a thin, textile-reinforced concrete shell built using a novel, ultra-lightweight, flexible formwork system. *1, 50-53.*

Veenendaal, D., Coenders, J., Vambersky, J., & West, M. (2011). Design and optimization of fabric-formed beams and trusses: evolutionary algorithms and form-finding. *12*(4).

Victoria, M., Querin, O. M., & Martí, P. (2011). Generation of strut-and-tie models by topology design using different material properties in tension and compression. *44:247–258.*

West, M. (2016). *The Fabric Formwork Book: Methods for Building New Architectural and Structural Forms in Concrete.* Routledge.

Yang, B., & Chen, C. (1996). Stress-based topology optimization. *12, 98-105.*

Yang, Y., Moen, C. D., & Guest, a. J. (2014). Three-Dimensional Force Flow Paths and Reinforcement Design in Concrete via Stress-Dependent Truss-Continuum Topology Optimization. *J. Eng. Mech*, 141(1): 04014106.

Zegard, T.́., & Paulino, G. H. (2016). Bridging topology optimization and additive manufacturing. *Struct Multidisc Optim*, 53:175–192.

Zhu, J.-H., Zhang, W.-H., & Xia, L. (2016). Topology Optimization in Aircraft and Aerospace Structures Design. *23:595–622.*